# Raypath Separation With a High-Resolution Algorithm in a Shallow-Water Waveguide

Longyu I Jiang, Philippe I Roux, Jerome I. Mars

# Raypath Separation with a High-Resolution Algorithm in a Shallow-Water Waveguide

Longyu Jiang, *Member, IEEE,* Philippe Roux,
and Jérôme I. Mars, *Member, IEEE,*

**Abstract**

One intriguing property that is exploited by ocean acoustic tomography (OAT) is that acoustic signals travel in a multipath. As the first step of OAT, each ray path should be identified with a particular travel time. However, the set of multipath rays generated by an emitted signal is correlated or coherent, as they are produced by reflection and or by refraction in propagation. In this paper, a high-resolution method called smoothing-Multiple Signal Classification Active Large Band (MUSICAL) is presented in the context of shallow-water OAT for separating coherent or fully correlated raypaths in the direction of arrival (DOA)-temporal domain. The method is a combination of the MUSICAL and spatial-frequency smoothing processing. Furthermore, the performance of smoothing-MUSICAL is illustrated by experiments based on both synthetic data and real data. This algorithm largely improves separation performances and presents fewer artifacts compared to conventional beamforming. In particular, experimental results show that smoothing-MUSICAL is more robust than beamforming facing a noisy environment with moderate signal-to-noise ratio (SNR).

**Index Terms**

Ocean acoustic tomography, Multipath propagation, Shallow-water waveguide, High resolution

Longyu Jiang is with the Laboratory of Image Science and Technology, Southeast University, Nanjing 210096, China; the Key Laboratory of Computer Network and Information Integration (Southeast University), Ministry of Education, China; and Centre de Recherche en Information Biomedicale Sino-Francais (LIA CRIBs), Rennes, France.

Philippe Roux is with Institut des Sciences de la Terre, Université Joseph Fourier, Centre National de la Recherche Scientifique, Unité Mixte de Recherche 5275, 1381 Rue de la Piscine, Saint-Martin d'Hères, France.

Jérôme I. Mars is with Laboratoire Grenoble Images Parole Signal Automatique, Institut Polytechnique de Grenoble, Centre National de la Recherche Scientifique, Unité Mixte de Recherche 5216, 961 Rue de la Houille Blanche, Saint-Martin d' Hères, France.

## I. INTRODUCTION

Ocean acoustic tomography (OAT) is a measurement technique to acquire information on temperatures and currents of oceans. It was first introduced to provide large-scale images of ocean sound-speed fluctuations using low-frequency acoustic waves [1], whereas shallow-water acoustic tomography (SWAT) at small scale has received more attention in recent years due to easier measurement of the environment parameters and simpler array deployments [2]–[4]. SWAT also takes advantage of the multi-path property of the wave field. This property allows the improvement of the quality of tomography, but it also produces interfering fields in both the time and frequency domains. Therefore, ray identification and arrival time estimation cannot be realized without using a specialized signal processing technology. There are two general kinds of technologies: (1) beamforming-like methods and (2) multiple signal classification-like algorithms [5].

As a classical method, beamforming is frequently used to separate raypaths, typically applied on a vertical receiver array at the reception, which records the signal emitted by a single emitter. Compared to the configuration of a single hydrophone receiver, a vertical receiver array will provide two significant benefits at the cost of somewhat increased receiver complexity [1]: vertical receiving arrays can improve the signal-to-noise ratio (SNR) as well as enable the separation of some raypaths that are not resolved in the time domain using the arrival angles. Although the advantages of using beamforming on a receiver array have been presented above, its major drawback is limited resolving ability. It is necessary to provide more separated raypaths to improve the possibilities to get satisfying tomography results. Recently, a tomography method has been developed using double beamforming to separate the different paths and extract more observations. Based on the principle of reciprocity, beamforming is applied twice to a configuration of array to array, which is composed of a vertical source array and a vertical array of receivers, once in the vertical array of emission and the other in reception. Because of exploiting the emission array, the emitted angle of each raypath is taken as an additional parameter to separate raypaths. Thus, double beamforming has improved the conventional beamforming performances [2]. However, it is still confronted with the main beamforming drawback: the low-resolution performance.

The stronger ability to distinguish closely spaced signals is referred to as ”high resolution”. The high-resolution method, referred to as the subspaced-based method [6], is another type of

well-known methods for source separation. Generally, it is based on a multi-path propagation model and takes advantage of the statistical properties of the received signal. Then, certain parameters such as the angle of reception and arrival time are estimated by maximizing or minimizing a function [7]–[10]. In particular, as the emitted signal is known, a Multiple Signal Classification Active Large Band (MUSICAL) algorithm [10] is introduced to separate close raypaths using the spectrum and module information of the emitted signal. MUSICAL performs better than beamforming under the assumption of decorrelated raypaths. However, multiple raypaths produced by the reflection of the emitted signal are fully correlated, and even coherent. In this case, the performance of MUSICAL with respect to source separation or the noise level drops sharply. Thus, it is crucial to present a high-resolution processing to separate the coherent or highly correlated raypaths in view of practical importance.

Although there is no application in the context of OAT, algorithms for separating coherent signals have been studied a lot in theory. Effective spatial smoothing has been developed for separating narrowband correlated sources: it was first studied by Evans et al. [11], [12]. A more complete analysis in conjunction with the eigenstructure technique is demonstrated by Shan et al. [13]. Then, it is extended to forward-backward spatial-smoothing approach by Rao and Hari [14]. Simulation results show that combining spatial smoothing with the forward-backward approach is more effective than using forward spatial smoothing alone. Because the conventional spatial smoothing leads to a reduction of the array aperture and a poorer direction of arrival (DOA) estimation, enhanced spatial smoothing methods are presented by Shan et al. [13] and Choi [15], which improve significantly the resolution of the conventional ones. Al-Ardi et al. [16] proposed an iterative spatial smoothing algorithm to reduce the computational cost of spatial smoothing, owing to the eigendecomposition of the array covariance matrix. By resolving uncorrelated and correlated signals separately, it is performed in two stages. In the first stage, it needs to form the uncorrelated signals covariance matrix, which is difficult in realization. Due to using only the forward spatial smoothing instead of the forward-backward spatial smoothing in the construction of the smoothed data matrix, the effective aperture of the array is largely reduced. Besides, a group of spatial smoothing methods is proposed for DOA estimation in the presence of correlated noise fields, such as a matrix decomposition method introduced by Rajagopal and Rao [17], a weighted spatial smoothing algorithm proposed by Tan and Oh [18], and a spatial difference smoothing method presented by Qi et al. [19].

Detecting multiple sources and estimating DOA are also emphasized in the case of wideband

correlated sources. For instance, coherent signal subspace processing for wideband signals is shown in the frequency domain by Wang and Kaveh [8]. Specifically, coherently constructed signal space results in an appropriately frequency-averaged estimate of the spatial covariance matrix. This estimate is statistically more accurate and, to a large extent, immune to the degree of correlation between the sources. Wang and Kaveh [20] analytically studied the performance of signal subspace processing for detecting multiple wideband sources.

Recently, Paulus and Mars [21] presented a method, called multicomponent wideband spectral matrix filtering, which is applied on geophysical data to separate interfering wave fields. The technique is based on the decomposition of a special multicomponent spectral matrix and could extract a given wave field from a multicomponent data set. Novel smoothing methods considered in spatial, frequency, and spatial-frequency domains are introduced to correctly estimate a multicomponent wideband spectral matrix. Inspired by these algorithms [21], in this paper, we propose a novel high-resolution processing [22] to identify coherent raypaths in a shallow-water waveguide. This novel processing called by smoothing-MUSICAL combines MUSICAL algorithm [10] and spatial-frequency smoothing and is performed in a point-array configuration. In addition, its resolution performances are compared to those of conventional beamforming processing based on simulations and experiments.

This paper is structured as follows: In Section 2, the signal model and the principle of smoothing-MUSICAL are introduced; In Section 3, (1) the performance of smoothing-MUSICAL is illustrated by synthetic data and (2) the results with low SNR simulation are shown to test the robustness of smoothing-MUSICAL. In Section 4, smoothing-MUSICAL is applied to real data obtained from a small-scale experiment.

## II. SMOOTHING-MUSICAL

High-resolution methods generally require an accurate modeling of the received signals exploiting information such as plane waves or uncorrelated sources. These signals are assumed to be random and stationary. High-resolution methods were first designed for passive antennas, with the assumption that there is no information on the temporal shape of the received signal. One of the easiest cases is to analyze that of narrowband signals. By taking into account the spectral range of the signal, the narrowband methods have been extended for application to wideband signals. However, by either a frequency analysis [8] or a temporal analysis [9] of the signal, these methods still only consider wideband signals as random ones and therefore do not provide information

on frequency characteristics (amplitude and phase spectrum) or time (waveform) signal. By taking advantage of the frequency characteristics, Gounon and Bozinoski [10] proposed an active wideband multiple signal classification algorithm using multiple realizations, and it lies in the assumptions of decorrelated sources. However, these assumptions are difficult to achieve in a practical shallow-water environment. Thus, we propose the smoothing-MUSICAL algorithm, which is based on a single realization and enables to separate the fully correlated or coherent raypaths. The algorithm is described in the following sections.

### A. *Signal model*

The signal model is built on an acoustic field composed of $P$ raypaths. These raypaths arrive on a vertical antenna of $M$ sensors. The temporal signal received on the $m^{th}$ sensor is modeled as

$$x_m(t) = \sum_{p=1}^{P} a_p e(t - \tau_{m,p}) + n_m(t) \tag{1}$$

where $x_m(t)$ is the received signal on the $m^{th}$ sensor, $e(t)$ is the signal emitted by the source, $a_p$ is the amplitude of the $p^{th}$ raypath on the $m^{th}$ sensor, and $n_m(t)$ is the additive noise received at the $m^{th}$ sensor. In frequency domain, (1) is written as

$$x_m(\nu) = \sum_{p=1}^{P} a_p e(\nu) \exp(-j2\pi\nu\tau_{m,p}) + n_m(\nu) \tag{2}$$

The arrival time $\tau_{m,p}$ can be expressed as follows

$$\tau_{m,p} = T_p + t_m(\theta_p) \tag{3}$$

Eq. (2) can be rewritten with Eq. (3) as follows

$$x_m(\nu) = \sum_{p=1}^{P} a_p e(\nu) \exp(-j\nu(\Psi_p + (m-1)\Phi_p)) + n_m(\nu) \tag{4}$$

with:

$$\Psi_p = 2\pi T_p \quad \Phi_p = 2\pi t_m(\theta_p)$$

where $T_p$ is the arrival time of the $p^{th}$ raypath on the reference sensor, and $t_m(\theta_p)$ is the delay between the reference sensor and the $m^{th}$ sensor. $t_m(\theta_p)$ is a function of $\theta_p$, which is the arrival direction of raypath on the antenna. $t_m(\theta_p)$ is a function of $\theta_p$, which is the arrival direction of the $p$th raypath on the antenna. In addition, $t_m(\theta_p) = \frac{dsin\theta_p}{c}$, where $d$ is the distance between two adjacent sensors. $c$ is the propagation velocity of the acoustic signal.

In Eq. (2), the term $e(\nu)$ is the deterministic amplitude of the emitted signal at the frequency $\nu$. The amplitude of each raypath $a_p$ is considered random and uncorrelated. Eq. (2) can be written as a matrix form using $F$ frequency bins of the signal:

$$\mathbf{x}_g = \mathbf{H}.\mathbf{A} + \mathbf{n}_g \tag{5}$$

where $\mathbf{x}_g = [\mathbf{x}^+(\nu_1), \mathbf{x}^+(\nu_2), \cdots, \mathbf{x}^+(\nu_F)]^+$ with $\mathbf{x}(\nu_i) = [x_1(\nu_i), x_2(\nu_i), \cdots, x_M(\nu_i)]^+$ is a vector of dimension $M \times F$ obtained by the concatenation of the observation vectors at each frequency, $F$ is the number of frequency bins of the signal, $\mathbf{n}_g = [\mathbf{n}^+(\nu_1), \mathbf{n}^+(\nu_2), \cdots, \mathbf{n}^+(\nu_F)]^+$ with $\mathbf{n}(\nu_i) = [n_1(\nu_i), n_2(\nu_i), \cdots, n_M(\nu_i)]^+$ is a vector of dimension $M \times F$ obtained by the concatenation of the observation of noise vectors at each frequency, $\mathbf{A} = [a_1, a_2, \cdots, a_P]^+$ is a vector of dimension $P$, $\mathbf{H} = [\mathbf{h}_1, \mathbf{h}_2, \cdots, \mathbf{h}_P]^+$ with $\mathbf{h}_p = [e(\nu_i)e^{-2i\pi\nu_1\tau_{1p}}, \cdots, e(\nu_F)e^{-2i\pi\nu_F\tau_{Mp}}]^+$, and $\mathbf{H}$ is a matrix of dimension $(M \times F, P)$. $\mathbf{H}$ puts together the terms $e^{-2i\pi\nu_1\tau_{mp}}$, which describes the transfer functions between the sources and the sensors, $e(\nu_i)$ characterizes the emitted signal, and $+$ means transposed.

### *B. Principle of the algorithm*

Based on the signal model described above, we will present the principle of the algorithm and the first step is to estimate interspectral matrix.

*1) Estimation of the interspectral matrix:* The interspectral matrix of the received data is computed by exploiting Eq. (5):

$$\mathbf{\Gamma} = E(\mathbf{x}_g\mathbf{x}_g^*) = \mathbf{H}\,\mathbf{\Gamma_C}\,\mathbf{H}^* + \mathbf{\Gamma_N} = \mathbf{\Gamma_Y} + \mathbf{\Gamma_N} \tag{6}$$

where * means transpose conjugated. $\mathbf{\Gamma_C}$ is the source correlation matrix in $P \times P$ dimension, $\mathbf{\Gamma_Y}$ is the nonnoisy wideband interspectral matrix, and $\mathbf{\Gamma_N}$ is the noise wideband interspectral matrix.

The rank of $\mathbf{\Gamma}$ must be at least equal to $P$ under the assumption of uncorrelated raypaths. MUSICAL could get effective separation in this case. However, in a practical experiment, a single realization and correlated raypaths inevitably lead to rank deficiency. Particularly, when the raypaths are fully correlated or coherent, the interspectral matrix will be a singular matrix and it is impossible to directly separate these raypaths with MUSICAL.

- Wideband spatial smoothing

Smoothing techniques are frequently used to increase the rank of the interspectral matrix. Although spatial and frequency smoothing techniques have been applied to narrowband signals, these methods cannot be directly extended to the active wideband case, as the nature and structure of interspectral matrices are indeed different.

Inspired by these narrowband algorithms, the proposed wideband spatial smoothing first divides the principal antenna, which is composed of $M$ sensors, into $2K_s+1$ partially overlapping subantenna with $M-2K_s$ successive sensors. The subantenna indexed by $k_s$ includes the sensors in the range of $[k_s, k_s+1, \cdots, k_s+M-2K_s]$. All of the signals received by $2K_s+1$ subantennas are exploited to compute the expectation of broadband spectral matrix $\mathbf{\Gamma}^{k_s}$ ($\mathbf{\Gamma}^{k_s} = E[\underline{\mathbf{x}}_{l,k_s}\underline{\mathbf{x}}^*_{l,k_s}]$). The smoothing spectral matrix is then defined as the arithmetic mean of these spectral matrices, as shown in Eq. 7.

$$\hat{\mathbf{\Gamma}} = (2K_s+1)^{-1} \sum_{k_s=1}^{2K_s+1} \underline{\mathbf{x}}_{g,k_s}\underline{\mathbf{x}}^*_{g,k_s} \tag{7}$$

These subarrays are supposed to be linear and uniform. Based on this assumption, the ray does not vary rapidly, especially, without amplitude fluctuations over the number of sensors in each subarray. It has been proven that if the number of subarrays is greater than or equal to the number of sources, then the spectral matrix is nonsingular. As an example, in Fig. 1, a uniform linear array with $M = 7$ identical sensors (1, ...,7) is divided into overlapping subarrays of size $M - 2K_s = 5$. The first subarray is composed of sensors indexed from 1 to 5; similarly, the second one is composed of sensors from 2 to 6, etc.

We still need to consider two essential problems given the particular structure of broadband spectral matrix. The first one is whether the undergone structural changes during smoothing are compatible with the broadband modeling methods. The second one concerns the rank that is affected by the source correlation matrices.

Actually, the transition from sensor $m$ to sensor $m+1$ results in an additional phase shift for each source $p$. Because the linear array is composed of equidistant sensors, the transition from the first subarray to the $k_s$ subarray can be modeled by introducing a matrix named $\mathbf{B}^{k_s}$. It includes the phase shifts of sources observed at $F$ frequencies. The matrix is in dimension $M.F \times P$, and Eq. (8) describes its generic term:

$$B_f^{k_s} = exp[-j\nu(k_s-1)\Phi_p] \tag{8}$$

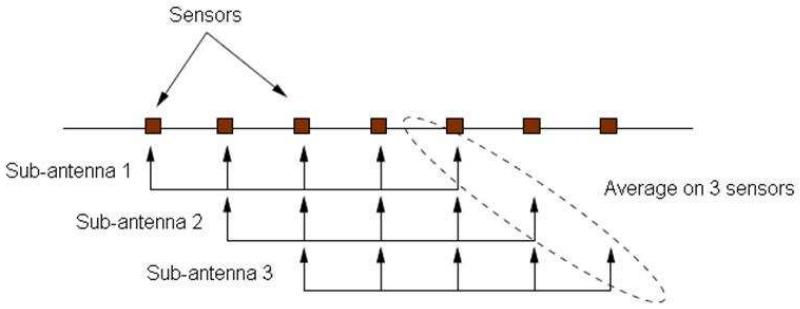


Fig. 1. Subantenna structure of spatial smoothing.

With these notations, the broadband observation vector of the subarray indexed by $k_s$ is written as

$$\underline{\mathbf{x}}_g^{k_s} = \mathbf{H}\mathbf{B}^{k_s}\mathbf{A} + \mathbf{N}^{k_s} \tag{9}$$

From this expression, the algebraic characterization of the transformations caused by broadband spectral matrices in the spatial smoothing can show that (1) the changes of spectral matrices due to smoothing are reduced essentially to a change in the source correlation matrix $\mathbf{\Gamma_C}$. (2) The rank augmentation of $\mathbf{\Gamma_C}$ depends on the number of sub-antennas $2K_s + 1$ and the number of coherent sources groups $Q$. It is equal to $(2K_s + 1) \times Q$. (3) The new ranks of $\mathbf{\Gamma_C}$ and $\mathbf{\Gamma_Y}$ are greater than or equal to $P$ when the condition $2K_s + 1 \geq \frac{P}{Q}$ is satisfied. (4) Finally, the ranks of the smoothing spectral matrix is increased by the value of $F \times P$.

These four items are sufficient to ensure that smoothing spectral matrices are similar to those that have been obtained with partially uncorrelated sources. In fact, they only express the decorrelation produced by smoothing processing. However, it should give special attention to the last two points and emphasize that it is not desirable to make a processed rank too large compared to $P$. In some situations, it may indeed lead to dysfunctions that are similar to those matrices encountered with nonsmoothing results during the excessive overestimation of the number of sources.

- Wideband frequency smoothing

A similar smoothing process as described in the previous paragraph can be applied in the frequency domain. This is largely due to the particular structure of the broadband observation vectors used by MUSICAL. Then, it is possible to introduce a frequency smoothing if the following two assumptions are met (1) there is a prior whitening of received signals and (2) frequency channels must be equally spaced on the analysis band. Similarly, frequency smoothing is performed by dividing the band composed of $F$ frequency channels into $2K_f + 1$ partially overlapping subbands of $F - 2K_f$ channels. Thus, the subband of index $k_f$ is composed of channels $[k_f, k_f + 1, \cdots, k_f + F - 2K_f]$. The spectral matrix of the observation is then defined as the average of the $2K_f + 1$ submatrices, as is shown in Eq. 10.

$$\hat{\mathbf{\Gamma}} = (2K_f + 1)^{-1} \sum_{k_f=1}^{2K_f+1} \underline{\mathbf{x}}_{g,k_f} \underline{\mathbf{x}}_{g,k_f}^{*} \tag{10}$$

$$B_m^k = exp[-j\Delta(k-1)(\Psi_p + (m-1)\Phi_p)] \tag{11}$$

Fig. 2 shows an example of frequential subband division for $F = 10$ and $K_f = 2$.

The $M^2$ blocks of the broadband smoothed spectral matrix in the frequency domain have quite similar properties and structure to those of $F^2$ blocks of the spatially smoothed matrix. The characteristics of frequency smoothing can be deduced from all of those obtained in the study of broadband spatial smoothing. It shows in particular that $2K_f + 1$ subbands are enough for estimating the ranks of $\mathbf{\Gamma_C}$ and $\mathbf{\Gamma_Y}$ when they are not larger than $(2K_f + 1) \times Q$.

- Spatial-frequency smoothing

The two methods discussed above may well obviously be used together and making a strong smoothing either in distance or in frequency may introduce a significant bias in the estimation of the matrix. To solve this problem, the combination of the two types of smoothing provides more flexibility in processing, particularly for the antennas that are composed of a limited number of sensors and for which the spatial smoothing methods are not applicable [21]. ($K_s$ and $K_f$ denote the spatial and frequency smoothing factor, respectively). From the single available observation $\underline{\mathbf{x}}$, by jointly using the two forms of smoothing, it is possible to generate a set of $(2K_s + 1)$ spatially recurrences $\underline{\mathbf{x}}_{g,k_s}$. These $2K_s + 1$ recurrences are then shifted frequentially to obtain

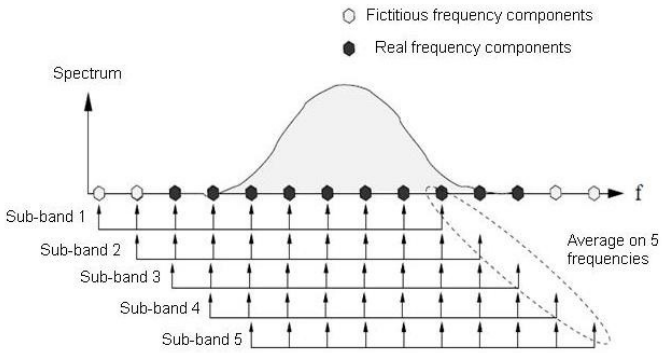


Fig. 2. Subband structure of the frequential smoothing.

$K = (2K_s+1)(2K_f+1)$ recurrences $\underline{\mathbf{x}}_{g,k_s,k_f}$. Finally, we can estimate the wideband interspectral matrix by the following formula:

$$\hat{\mathbf{\Gamma}} = [(2K_s+1)(2K_f+1)]^{-1} \sum_{k_s=1}^{2K_s+1} \sum_{k_f=1}^{2K_f+1} \underline{\mathbf{x}}_{g,k_s,k_f} \underline{\mathbf{x}}_{g,k_s,k_f}^{*} \tag{12}$$

The rank of the interspectral matrix thus estimated is equal to $K$. To achieve an effective separation of raypaths and noise, it is necessary to select $K$ greater than $P$.

*2) Estimation of the signal subspace:* Using the above spatial-frequency smoothing, the wideband interspectral matrix is estimated as $\hat{\mathbf{\Gamma}}$. Due to the assumptions that the sources and the noise are uncorrelated, $\hat{\mathbf{\Gamma}}$ is decomposed as

$$\hat{\mathbf{\Gamma}} = \hat{\mathbf{\Gamma}}_{\mathbf{s}} + \hat{\mathbf{\Gamma}}_{n} \tag{13}$$

Because the spectral matrix has a Hermitian symmetry:

$$\hat{\mathbf{\Gamma}} = \hat{\mathbf{\Gamma}}^{*} \tag{14}$$

It can be decomposed in a single way using eigenvector decomposition (EVD) as

$$\begin{aligned}\hat{\mathbf{\Gamma}} &= U \wedge U^* \\ &= \textstyle\sum_{k=1}^{MF} \lambda_k \mathbf{u_k} \mathbf{u_k}^* \\ &= \textstyle\sum_{k=1}^{P} \lambda_k \mathbf{u_k} \mathbf{u_k}^* + \sum_{k=P+1}^{MF} \lambda_k \mathbf{u_k} \mathbf{u_k}^*\end{aligned} \tag{15}$$

where $\wedge = diag(\lambda_1, \ldots, \lambda_M)$ are the eigenvalues and $U$ is a unitary $(M \times F)$ by $(M \times F)$ matrix whose columns are the orthonormal eigenvectors $\mathbf{u}_1$, ..., $\mathbf{u}_M$ of $\hat{\mathbf{\Gamma}}$. The eigenvalues $\lambda_i$ correspond to the energy of the data associated with the eigenvalue $u_i$. They are arranged as follows:

$$\lambda_1 \geq \lambda_2 \geq \cdots \geq \lambda_M \geq 0$$

Based on the above eigendecomposition, the signal subspace is spanned by the first $P$ eigenvectors of $\hat{\mathbf{\Gamma}}$, and its complementary, the noise subspace is spanned by the orthogonal $MF - P$ last eigenvectors. The orthogonal projection onto the noise subspace is estimated as:

$$\hat{\mathbf{\Gamma}_n} = \sum_{k=P+1}^{MF} \mathbf{u_k} \mathbf{u_k}^* \tag{16}$$

Finally, the high-resolution algorithm consists of maximizing the following function:

$$F(\theta, T) = \frac{1}{\mathbf{a}(\theta, T)^* \, \hat{\mathbf{\Gamma}_n} \, \mathbf{a}(\theta, T)} \tag{17}$$

The wideband steering vector $\mathbf{a}(\theta, T)$ is the concatenation of the vectors $\mathbf{d}(\nu_i, \theta)$, which is the classical steering vector used in narrowband analysis. It is written as follows:

$$\mathbf{a}(\theta, T) = \begin{bmatrix} e(\nu_1) e^{-2i\pi\nu_1 T} \mathbf{d}^+(\nu_1, \theta) \\ \cdots \\ e(\nu_F) e^{-2i\pi\nu_F T} \mathbf{d}^+(\nu_F, \theta) \end{bmatrix}$$

with:

$\mathbf{d}(\nu_i, \theta) = [1, e^{-2i\pi\nu_i \tau_{1,2}(\theta)}, \ldots, e^{-2i\pi\nu_i \tau_{1,M-1}(\theta)}]^+$

$\mathbf{d}(\nu_i, \theta)$ contains the informations concerning the phase shifts between sensors at a given frequency and for a raypath with arrival angle $\theta$.

### C. Model error analysis

The model errors discussed in this paper include the effects of imprecisely known sensor location, perturbations in the antenna amplitude and phase pattern, and so on. These errors introduce subspace perturbations, which finally cause estimation errors of the arrival times and the directions of the arrivals. We assume the data matrix $\mathbf{X}_g = [\mathbf{x}_g(1), \mathbf{x}_g(2), \cdots, \mathbf{x}_g(L)]$ with $L$ as the number of samples used in experiments. We obtain the subspace decomposition equivalently by a singular value decomposition (SVD) on the data matrix $\mathbf{X}_g$.

$$\mathbf{X}_g = \mathbf{U}\mathbf{\Lambda}\mathbf{V}^* = [\mathbf{U}_s \quad \mathbf{U}_n] \begin{bmatrix} \mathbf{\Lambda_s} & \mathbf{0} \\ \mathbf{0} & \mathbf{0} \end{bmatrix} \begin{bmatrix} \mathbf{V}_s{}^* \\ \mathbf{V}_n{}^* \end{bmatrix} \tag{18}$$

where $U_s$ represents the singular vectors corresponding to the $P$ largest singular values, whereas $U_n$ represents the singular vectors corresponding to the noise singular value. Thus, a perturbation matrix $\Delta\mathbf{X}_g$ induces errors in the estimation of the perturbations of the $pth$ arrival time and the arrival direction of the $p$ th arrivals approximating as [10]

$$\Delta\theta_p = \hat{\theta}_p - \theta_p = \frac{\Re[\beta_{\mathbf{p}}{}^* \Delta\mathbf{X}_g{}^* \alpha_{1p}]}{\gamma_p} \tag{19}$$

$$\Delta T_p = \hat{T}_p - T_p = \frac{\Re[\beta_{\mathbf{p}}{}^* \Delta\mathbf{X}_g{}^* \alpha_{2p}]}{\gamma_p} \tag{20}$$

where

$$\beta_p = \mathbf{V}_s \mathbf{\Lambda}_s{}^{-1} \mathbf{U}_s{}^* \mathbf{a} \tag{21}$$

$$\alpha_{1p} = \frac{\mathbf{a}_T{}^* \mathbf{U}_n \mathbf{U}_n{}^* \mathbf{a}_T}{\Re[\mathbf{a}_\theta^* \mathbf{U}_n \mathbf{U}_n{}^* \mathbf{a}_T]} \mathbf{U}_n \mathbf{U}_n{}^* \mathbf{a}_\theta - \mathbf{U}_n \mathbf{U}_n{}^* \mathbf{a}_T \tag{22}$$

$$\alpha_{2p} = \frac{\mathbf{a}_\theta{}^* \mathbf{U}_n \mathbf{U}_n{}^* \mathbf{a}_\theta}{\Re[\mathbf{a}_\theta^* \mathbf{U}_n \mathbf{U}_n{}^* \mathbf{a}_T]} \mathbf{U}_n \mathbf{U}_n{}^* \mathbf{a}_T - \mathbf{U}_n \mathbf{U}_n{}^* \mathbf{a}_\theta \tag{23}$$

$$\gamma_p = \frac{\mathbf{a}_T{}^* \mathbf{U}_n \mathbf{U}_n{}^* \mathbf{a}_T \mathbf{a}_\theta{}^* \mathbf{U}_n \mathbf{U}_n{}^* \mathbf{a}_\theta}{\Re[\mathbf{a}_\theta^* \mathbf{U}_n \mathbf{U}_n{}^* \mathbf{a}_T]} - \Re[\mathbf{a}_\theta^* \mathbf{U}_n \mathbf{U}_n{}^* \mathbf{a}_T] \tag{24}$$

$$\mathbf{a}_\theta = \frac{\partial \mathbf{a}}{\partial \theta}(\theta_p, T_p) \tag{25}$$

$$\mathbf{a}_T = \frac{\partial \mathbf{a}}{\partial T}(\theta_p, T_p) \tag{26}$$

## III. Simulations

### A. Configuration

The performance of the proposed method is illustrated in this section. The simulation data is built using parabolic propagation equations [23], [24]. The sampling frequency of the emitted signal is 10,400 Hz and the bandwidth is 600 Hz. Our experiment equipment is composed of one source and a vertical array of 61 receivers. The source is fixed at 64 m under the ocean. The 61 receivers are regularly spaced in the water column between 49 and 79 m. We choose the 31st sensor as the reference one. The distance between the source and the reference sensor is 2 km. The configuration is shown in Fig. 3. The sampling frequency and the central frequency of the emitted signal are 10,400 and 1000 Hz, respectively. Raypaths propagate between the source and a receiver of the receiving array. Then, 1040 samples are used in the simulation.

### B. Results

We take conventional beamforming [25], [26] as a comparative method and both methods are tested through the same group of synthetic data.

The separation results of beamforming are presented in Fig. 4(a), whereas the ones of smoothing-MUSICAL are shown in Fig. 4 (b). Both methods identify the raypaths in a plan of reception angle and propagation time. In addition, each of the visible spots in Figs. 4 (a) and 4 (b) corresponds to the arrival of a raypath with its propagation time and the angle of reception. Black crosses are added in Figs. 4 (a) and 4 (b) to mark the theoretical positions of raypaths. Note that there are some biases in the peak location contained in Figs. 4 (a) and 4 (b). In practice, factors such as quantization, clock jitter, and other sources of noise make it virtually impossible for beamforming to realize the desired phase shifts. In Fig. 4(a), these biases of beamforming are mainly produced due to the quantization errors [27], [28]. In Fig. 4 (b), they

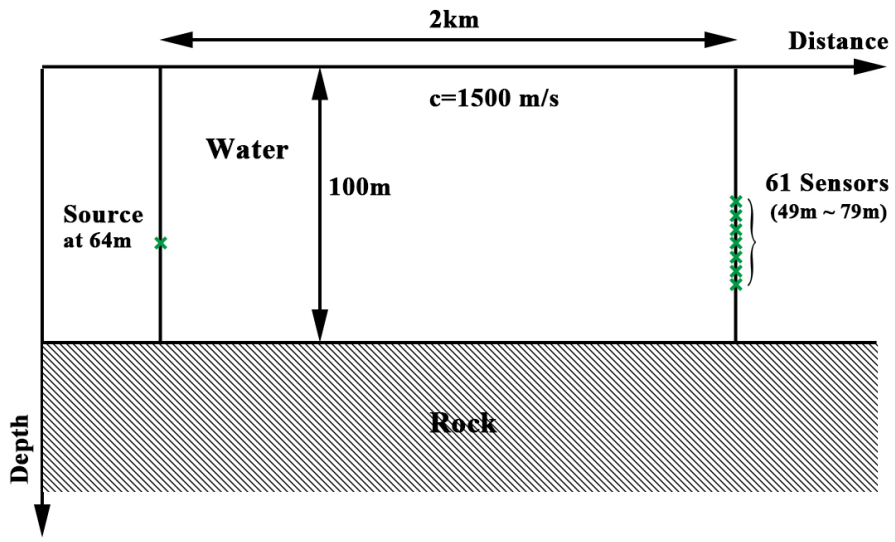


Fig. 3. Configuration of the simulations. One source is fixed at 64 m under the ocean. The 61 receivers are regularly spaced in the water column between 49 and 79 m. The distance between the source and the reference sensor is 2 km. The depth of the waveguide is 100 m.

are mainly produced by an uncompleted separation of signal and orthogonal subspaces when only finite samples are available in practice. An analytical expression relating the perturbations in the estimated orthogonal subspace to perturbations in the arrival directions and the arrival times has been derived by Wang and Kaveh [8]. Stoica and Arye [29] and Stoica and Nehorai [30] pointed out that high-resolution methods asymptotically reach the lowest mean square errors by the Cramer-Rao bound. However, the separation ability of beamforming is limited by the number of available sensors. Similarly, for large-length samples, the proposed algorithm produces less errors than beamforming, whereas beamforming gives relatively high errors or is even not able to resolve the early arrivals. This theoretical analysis is illustrated in Figs. 4(a) and 4(b). More precise results are obtained in Fig. 4(b). In particular, in Fig. 4(a) the proposed processing can separate first and the second raypaths, whereas, in Fig. 4(b), they are shown as a mixed point. In Fig. 4(b), the early arrivals appear to be about 6 dB lower than the late arrivals, as the array manifold vectors for the early arrivals are less orthogonal than the estimated noise subspace. This orthogonality derogation is also produced by the uncompleted separation of signal and noise subspaces. The better performance of the proposed high-resolution method is also based on the larger number of samples used in the estimation.

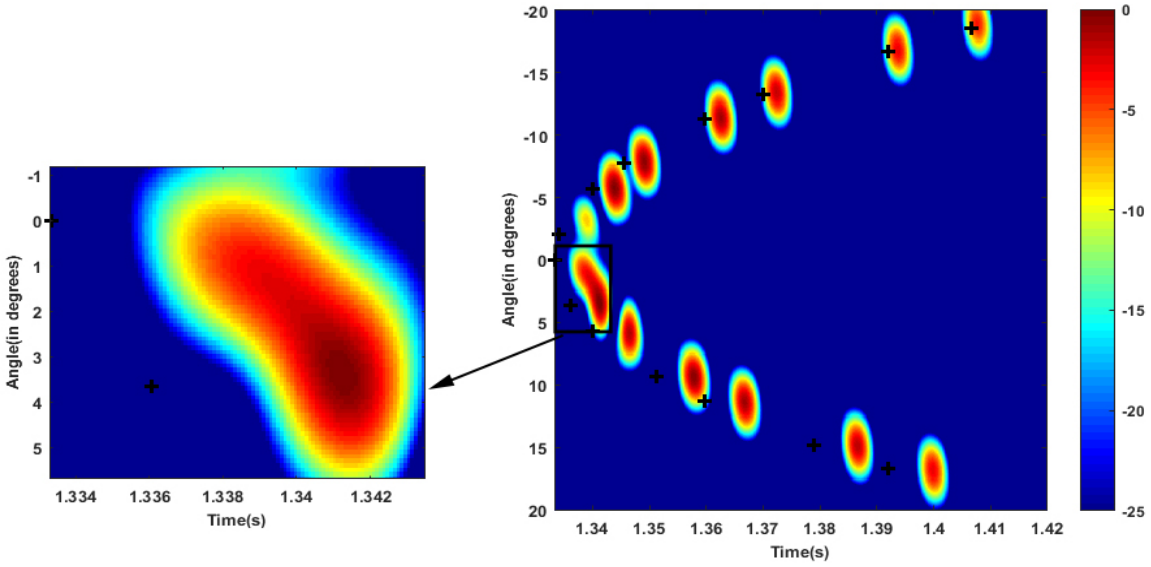


(a)

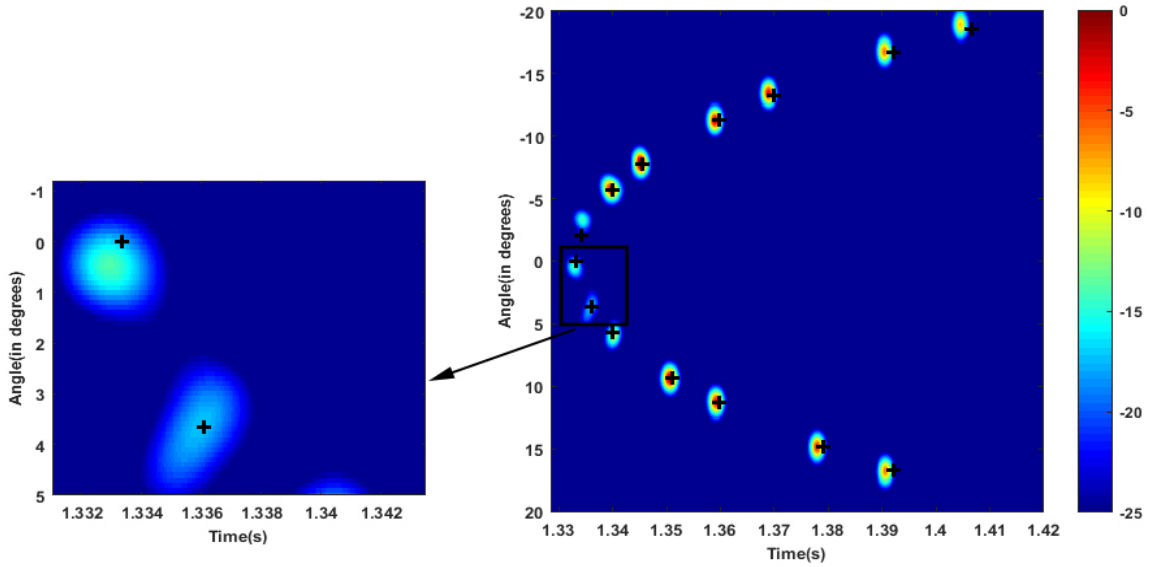


(b)

Fig. 4. Comparison of the results when the source is fixed at 64 m and the raypaths arrive on a vertical array composed of 61 sensors, which are regularly spaced in the water column between 49 and 79 m. Black crosses show the theoretical positions of the raypaths. (a) Separation results and the cross-section of the first two arrivals using the beamforming algorithm. (b) Separation results and the cross-section of the first two arrivals using the smoothing-MUSICAL algorithm.

### *C. Robustness against noise*

The identification ability of smoothing-MUSICAL under noiseless circumstances has been compared to that of beamforming in the above part. In this subsection, we will evaluate its

robustness to noise based on simulations with different SNRs. In these simulations, white Gaussian noise has been only added to the frequency band that the emitted signal occupies. Thus, the SNR is defined as the ratio of signal power to the noise power in the frequency band of the signal. Then, 312 samples are used in these simulations. The results for different SNRs are presented as follows:

SNR = 0 dB: Fig. 5 shows the received signals on the 61 received sensors when the SNR is equal to 0 dB. Fig. 6(a) shows the results obtained by beamforming. In this case, it cannot totally separate the first four raypaths. At the same time, separate results of smoothing-MUSICAL are shown in Fig. 6(b). Corresponding spots are visible and separate in the DOA-temporal domain. Similarly, observation noise results in the perturbation of estimated subspaces when only finite samples are available. In Fig. 6(b), this produces estimation errors of the arrivals and results in a reduced level of early arrivals by causing an incomplete separation of the two subspaces. Separation results obviously present more artifacts and larger estimation errors in Fig. 6(a) than the ones in Fig. 6(b). Compared to beamforming, smoothing-MUSICAL can effectively limit the influence of noise in the data when SNR = 0 dB.

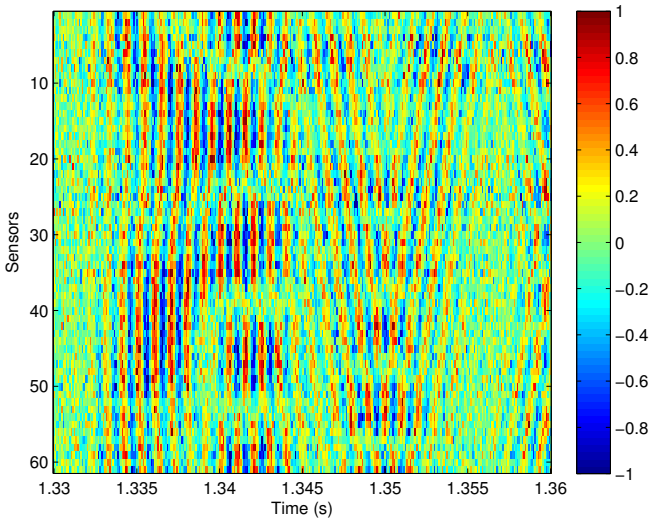


Fig. 5. Recorded signal (SNR = 0 dB)

SNR = -5 dB: When the SNR is equal to -5 dB, the ocean is a strongly noisy environment. The received signals with SNR = -5 dB are demonstrated in Fig. 7. Same as in the previous case, beamforming and smoothing-MUSICAL are respectively applied to the received signal. Marks

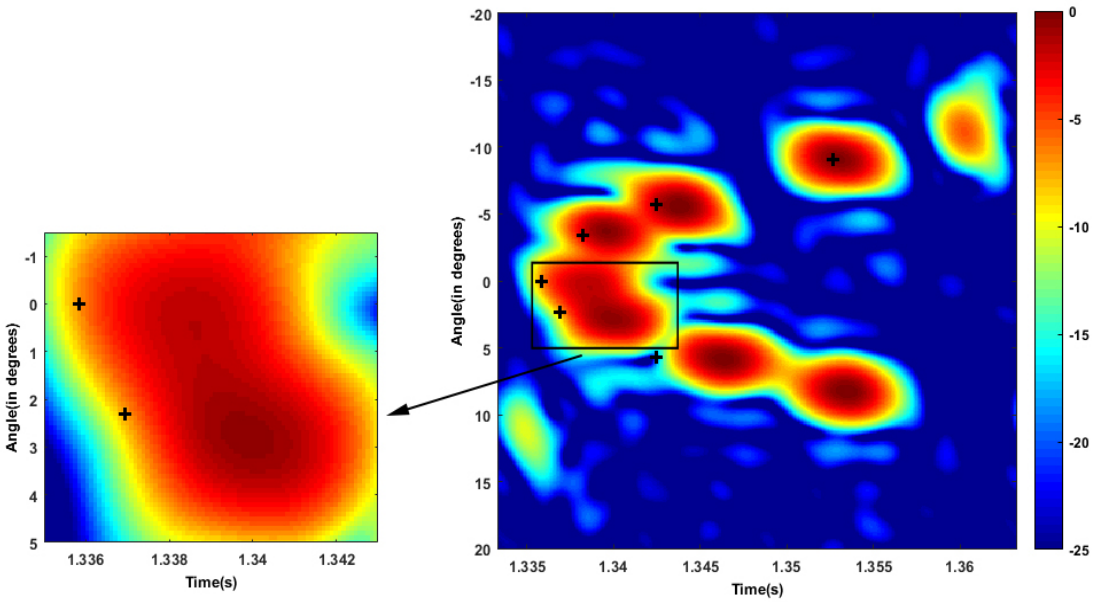


(a)

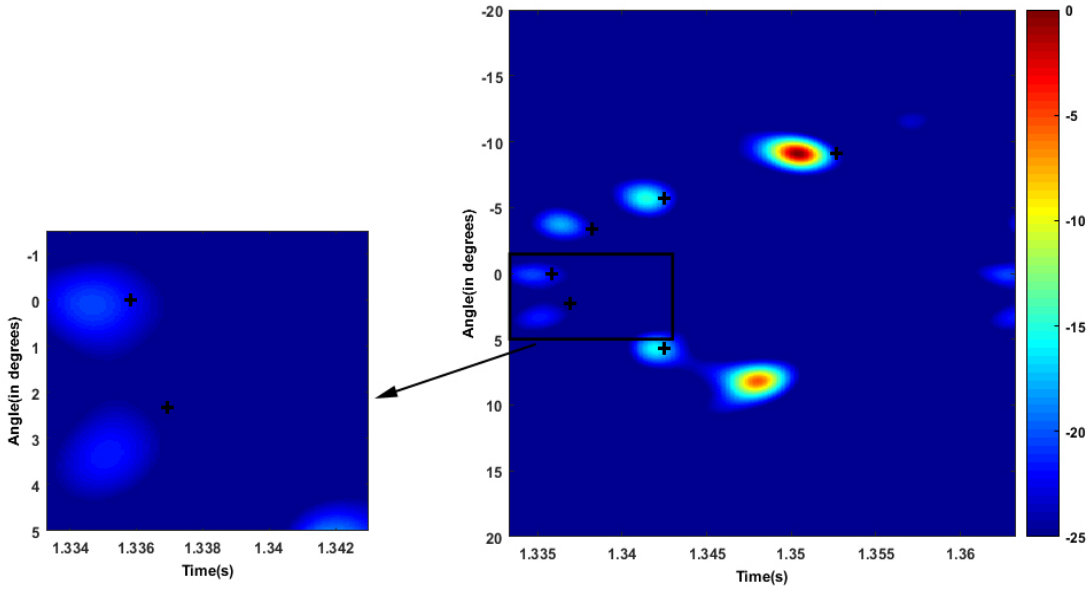


(b)

Fig. 6. Comparison of the results using 312 samples, where the SNR is equal to 0 dB. Black crosses indicate the theoretical positions of the raypaths. (a) Separation results and the cross-section of the first two arrivals using the beamforming algorithm. (b) Separation results and the cross-section of the first two arrivals using the smoothing-MUSICAL algorithm.

have been added in Figs. 8(a) and 8(b) to show the correct time and angle. Comparing Figs. 8(a) and 8(b), the first four raypaths are not distinct from Fig. 8(a) and there are some peaks missing from Fig 8(b). Both Figs. 8(a) and 8(b) show some errors and artifacts. Both algorithms

produce part of the useful results for SNR = -5 dB; however, the proposed algorithm did not provide better performance in view of robustness to noise.

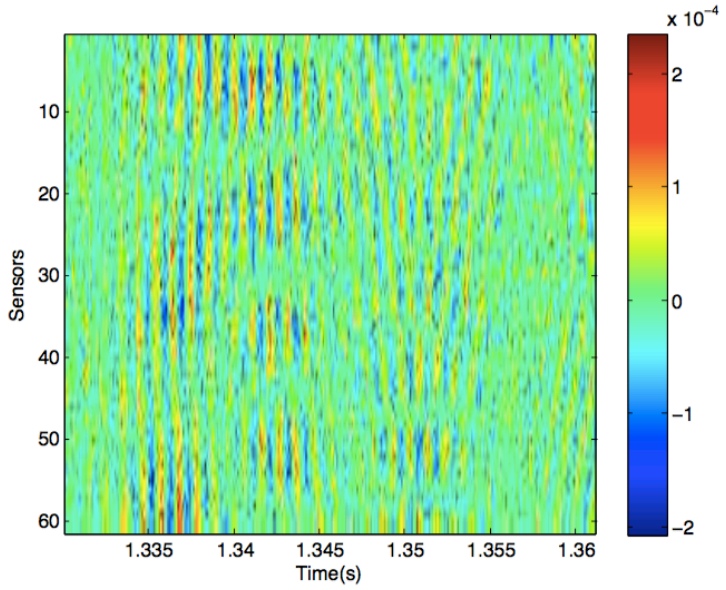


Fig. 7. Recorded signal (SNR = -5 dB).

## IV. Application on Real Data

A small-scale experiment is discussed in this part, so that we can further illustrate the performance of the proposed method. The principle on which this experiment is based is as follows: if the frequency of the signals is multiplied by a factor and the spatial distances, including both the one between the source and the receivers and the one between the adjacent receivers, are divided by the same factor, the physical phenomena occurring in the environment remain the same. Namely, the small-scale experiment reproduces the actual physical phenomena occurring in nature in a smaller scale inside the laboratory. It achieves a reduced cost and a totally controlled experiment. The experiment presented here was performed at the Institut des Sciences de la Terre (ISTerre) lab in the ultrasonic tank, which is developed by P. Roux. In this tank, a waveguide of 5 to 10 cm in depth and 1 to 1.5 m in length is constructed. A steel bar acts as the bottom, which is very reflective and perfectly flat. We will offer two experiments in the following section. The first experiment mainly shows the general performance of the proposed algorithm, whereas the second one focuses on illustrating the ability of separating close arrivals.

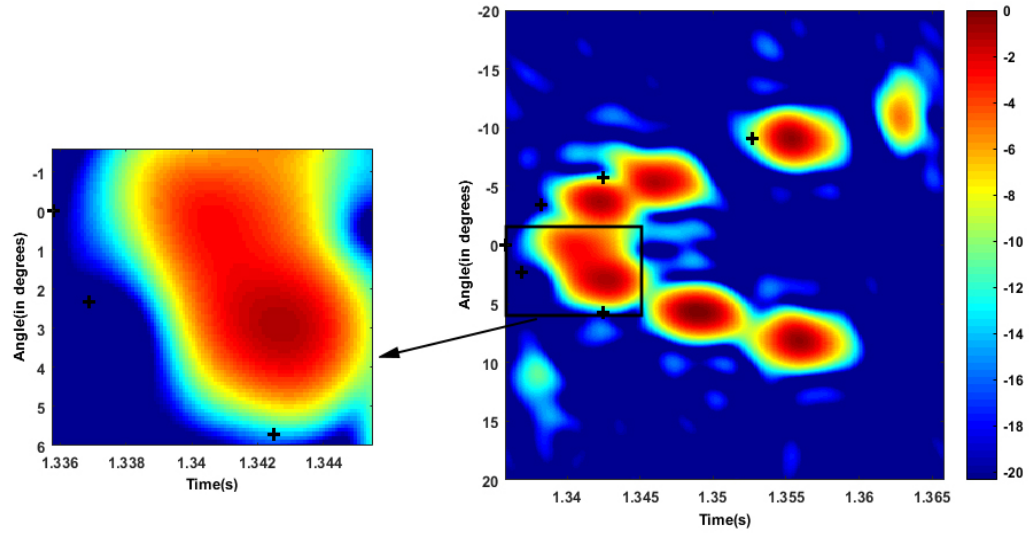


(a)

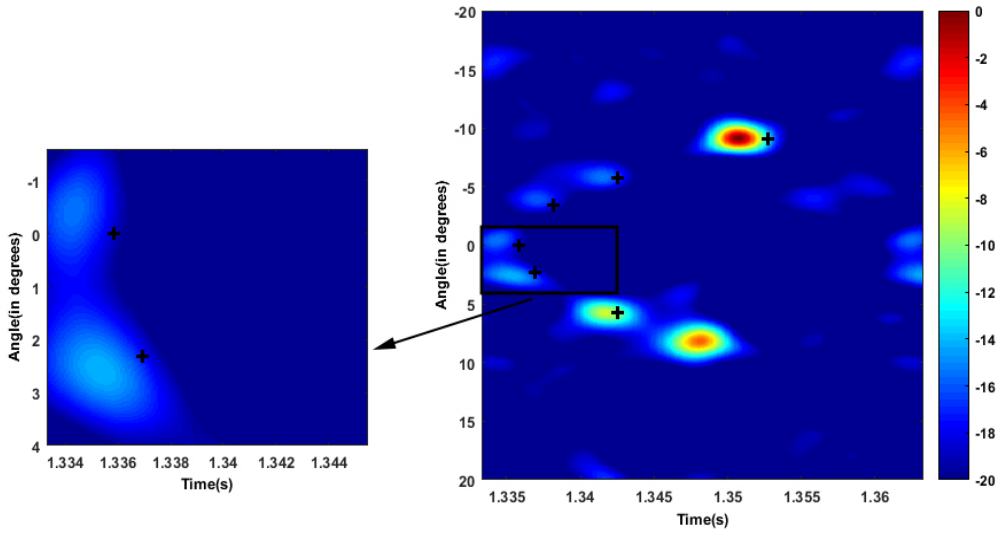


(b)

Fig. 8. Comparison of the results using 312 samples, where the SNR is equal to -5 dB. Black crosses show the theoretical positions of the raypaths. (a) Separation results and the cross-section of the first two arrivals using the beamforming algorithm. (b) Separation results and the cross-section of the first two arrivals using the smoothing-MUSICAL algorithm.

## A. *Experiment 1*

In the first experiment, a sensor is set at 0.0263 m in depth as an emitter. A vertical array composed of 64 sensors is taken as a reception. The depth of the first receiver is $3.55 \times 10^{-3}$ m.

The interval of two adjacent receivers is $0.75 \times 10^{-3}$ m. The distance between the emitter and the reference receiver is 1.1437 m. The water depth is 5.2 cm and the source signal with a 1 MHz frequency bandwidth has a central frequency of 1.2 MHz. The first 760 points in the time domain of the received signal with sampling frequency $F_e = 50$ MHz are used in this experiment. The recorded signals can be observed in Fig. 9. Separate results obtained by conventional beamforming are shown in Fig. 10(a). Beamforming detects six raypaths successfully, but it fails in totally separating the first two raypaths. For the same data, smoothing-MUSICAL (Fig. 10b) enables separating all the raypaths with precise physical position in the plan of DOA and arrival time.

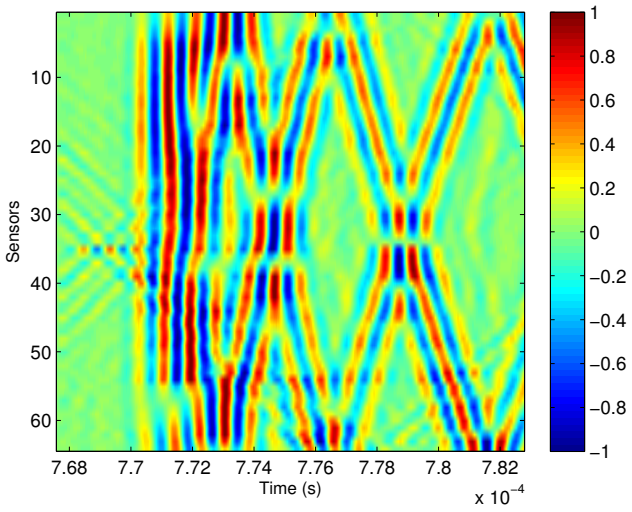


Fig. 9. Recorded signal for real data obtained at small scale.

Marks have been put at the location of the correct time and angle for all arrivals on both Figs. 10(a) and 10(b). The array manifold vectors for the early and the late arrivals have almost the same orthogonality to the noise subspace. Thus, the level of the early arrivals is not attenuated so much.

Limited resolution is always defined as the limited ability to determine a plane wave's direction of propagation and to separate two plane waves propagating in slightly different directions [31]. We can assess how well an array can localize a given source by the first definition. The second definition indicates how well sources can be distinguished. In this paper, we mainly focus on resolution given by the second definition. It is measured by using the temporal and angular width of the arrival peaks. Actually, we only consider the raypaths that can be well separated

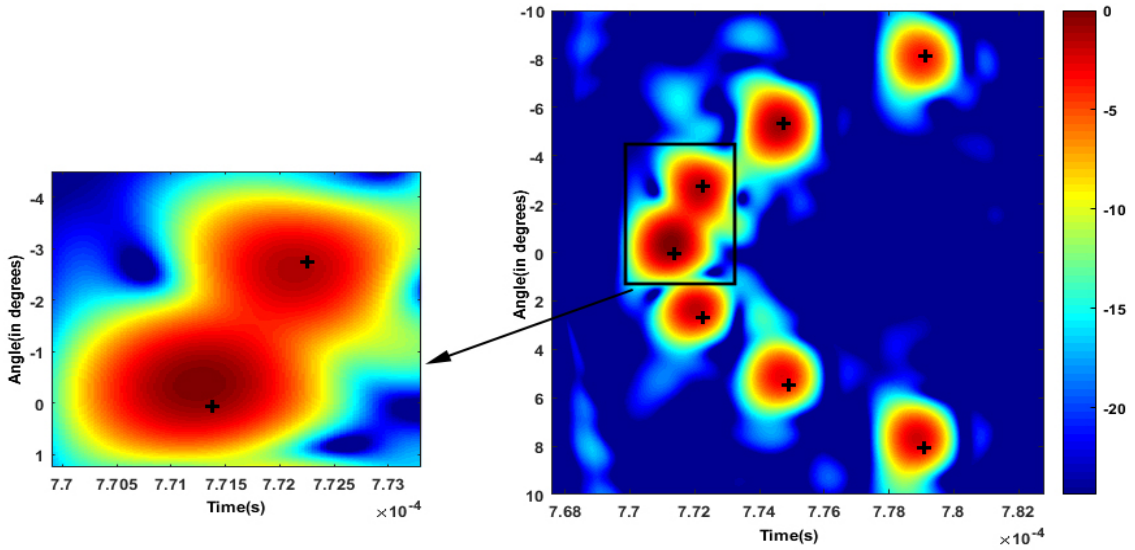


(a)

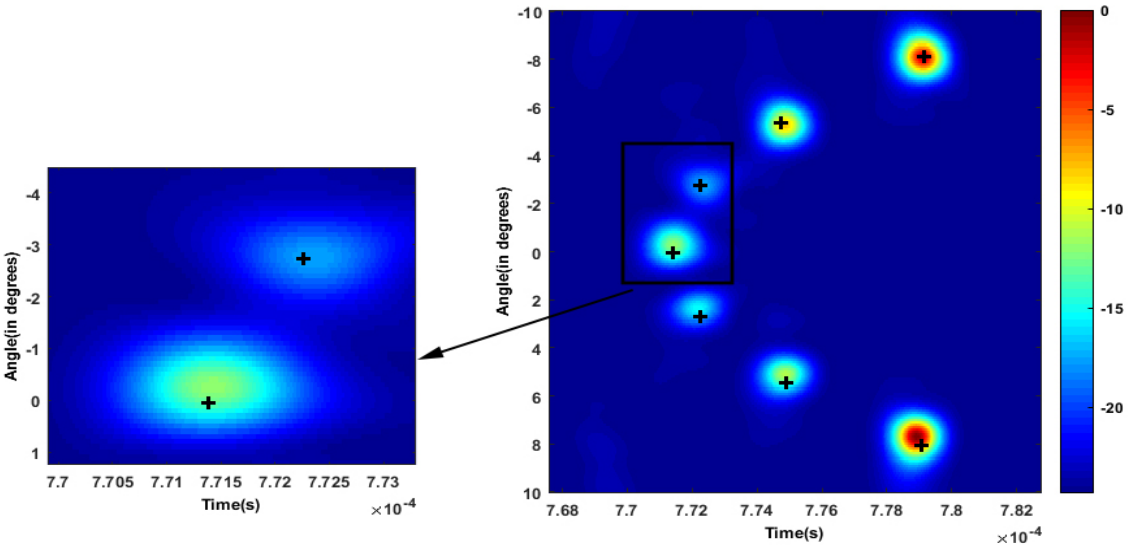


(b)

Fig. 10. Comparison of the results in the case of using real data obtained at small scale when the source is fixed at 26.3 mm under the water and the 64 sensors are regularly spaced in the water column between 35 and 75 mm. Black crosses indicate the theoretical positions of the raypaths. (a) Separation results using the beamforming algorithm and the cross-section of the first two arrivals. (b) Separation results using the smoothing-MUSICAL algorithm and the cross-section of the first two arrivals.

by both the smoothing-MUSICAL algorithm and the beamforming algorithm because the low resolution finally leads to two points can not be separated at all (a mixed point). However,

bias comparison according to the first definition is also considered. We refer to these raypaths in Figs. 10(a) and 10(b) from left to right successively. The comparisons of the results based on the second definition of time resolution and angle resolution are shown in Tables I and II, respectively. The comparisons of the results based on the first definition is given in Table III. Thus, we draw a conclusion that resolution improvements are largely made by the proposed algorithm.

TABLE I

TIME RESOLUTION COMPARISON

| Raypath | Beamforming ($\times 10^{-4}$ s) | Smoothing-MUSICAL ($\times 10^{-4}$ s) | Resolution increase(%) |
|---|---|---|---|
| 3 | 0.011 | 0.006 | 45.45 |
| 4 | 0.013 | 0.009 | 30.77 |
| 5 | 0.012 | 0.009 | 25.00 |
| 6 | 0.012 | 0.010 | 16.70 |
| 7 | 0.013 | 0.011 | 15.38 |

TABLE II

ANGLE RESOLUTION COMPARISON (°)

| Raypath | Beamforming | Smoothing-MUSICAL | resolution increase(%) |
|---|---|---|---|
| 3 | 1.43 | 0.7 | 51.05 |
| 4 | 1.55 | 0.85 | 45.16 |
| 5 | 1.61 | 0.75 | 53.42 |
| 6 | 1.56 | 0.9 | 42.31 |
| 7 | 1.54 | 0.95 | 38.31 |

## *B. Experiment 2*

In the second experiment, we fixed an emitter at 28.625 mm under the water. The interval of two adjacent receivers is $0.75 \times 10^{-3}$m. Twenty-one sensors are regularly spaced in the water column between 21.125 and 36.125 mm. The distance between the emitter and the reference receiver is 1 m and the source signal with a 1 MHz frequency bandwidth has a central frequency of 1.2 MHz. The first 150 points in the time domain of the received signal with sampling

TABLE III

RESOLUTION COMPARISON (IN $10^{-4}$SECONDS)

| Raypath | Beamforming (angle, time) | Smoothing-MUSICAL (angle, time) | Errors of beamforming (angle, time) | Errors of smoothing-MUSICAL (angle, time) |
|---|---|---|---|---|
| 3 | (2.33, 7.72 $\times 10^{-4}$) | (2.4, 7.72 $\times 10^{-4}$ ) | (0.363, 0.002$\times 10^{-4}$) | (0.296, 0.002$\times 10^{-4}$) |
| 4 | (-5.25, 7.746 $\times 10^{-4}$) | (-5.3, 7.749 $\times 10^{-4}$) | (0.102, 0.001$\times 10^{-4}$) | (0.052, 0.002$\times 10^{-4}$) |
| 5 | (5.11, 7.747 $\times 10^{-4}$) | (5.1, 7.749 $\times 10^{-4}$) | (0.366, 0.002$\times 10^{-4}$) | (0.376, 0) |
| 6 | (-8.06, 7.79 $\times 10^{-4}$) | (-8.1, 7.791 $\times 10^{-4}$) | (0.049, 0.001$\times 10^{-4}$) | (0.009, 0) |
| 7 | (7.69, 7.789 $\times 10^{-4}$) | (7.7, 7.789 $\times 10^{-4}$) | (0.384, 0.002$\times 10^{-4}$) | (0.374, 0.002$\times 10^{-4}$) |

frequency $F_e = 10MHz$ are used in this experiment. The separation results are shown in the Figs. 11(a) and 11(b). In addition, cross-sections are shown on the left of the figures.

In Figs. 11(a) and 11(b), the proposed processing manages to separate the second and the third raypaths, with the value of arrival time and the angle of reception as $(T, \theta) = (6.817 \times 10^{-4}, -2.75°)$ and $(T, \theta) = (6.817 \times 10^{-4}, 3°)$. However, in that case, beamforming presents us only one mixed spot.

## V. CONCLUSION

We propose the smoothing-MUSICAL algorithm to separate highly correlated or coherent raypaths in a shallow-water wave guide. The point-array configuration is considered to separate more raypaths by providing an arrival angle as a discriminating parameter. Compared to beamforming, the proposed processing has a better separation of raypaths with less noise artifacts and accurate physical position, particularly for the close raypaths. In the future, it will be applied to real acoustic signals in a 2D configuration composed of an array in emission and an array in reception.

## ACKNOWLEDGMENT

The work was supported by the National Natural Science Foundation of China (No. 61401085), the State Key Laboratory of Acoustics, Chinese Academy of Sciences (No. SKLA201604), the Scientific Research Foundation for the Returned Overseas Chinese Scholars.

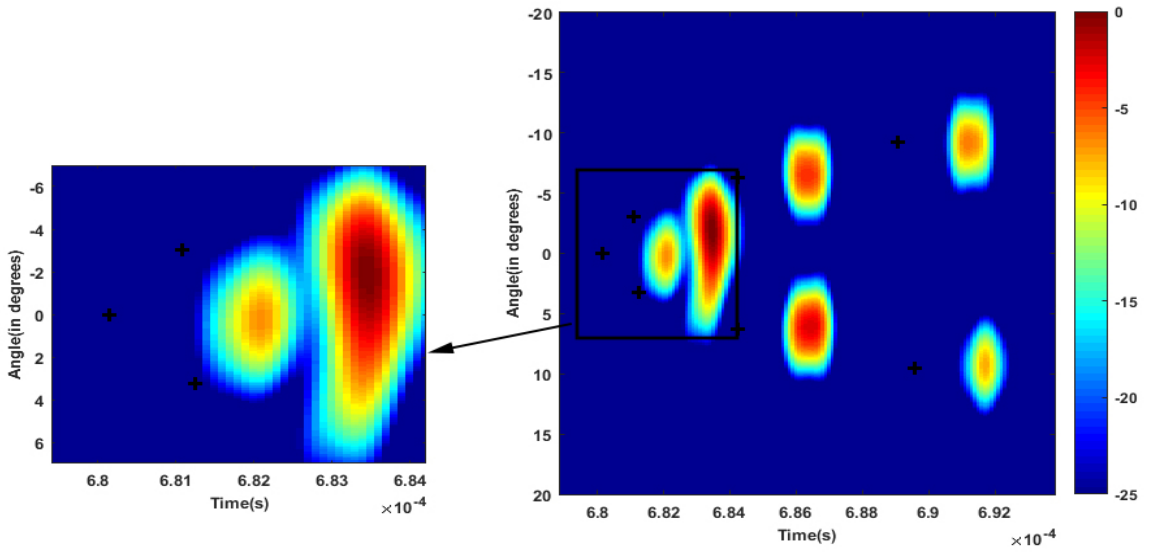


(a)

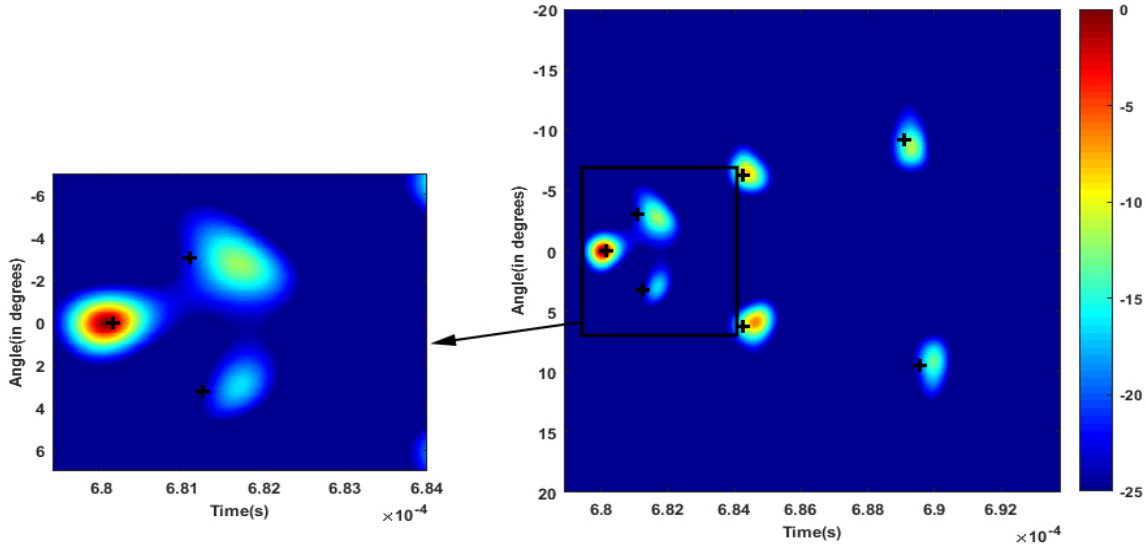


(b)

Fig. 11. Comparison of the results in the case of using real data obtained at small scale when the source is fixed at 28.625 mm under the water and the 21 sensors are regularly spaced in the water column between 21.125 and 36.125 mm. Black crosses indicate the theoretical positions of the raypaths. (a) Separation results using the beamforming algorithm and the cross-section of the first three arrivals. (b) Separation results using the smoothing-MUSICAL algorithm and the cross-section of the first three arrivals.

## REFERENCES

[1] W. Munk, P. Worcester, and C. Wunsch, *Ocean Acoustic Tomography*. Cambridge University Press, 1995.

[2] I. Iturbe, P. Roux, B. Nicolas, J. Virieux, J. Mars *et al.*, "Shallow-water acoustic tomography performed from a double-beamforming algorithm: simulation results," *Oceanic Engineering, IEEE Journal of*, vol. 34, no. 2, pp. 140–149, 2009.

[3] P. Roux, W. Kuperman, W. Hodgkiss, H. Song, T. Akal, and M. Stevenson, "A nonreciprocal implementation of time reversal in the ocean," *The Journal of the Acoustical Society of America*, vol. 116, p. 1009, 2004.

[4] P. Roux, I. Iturbe, B. Nicolas, J. Virieux, and J. Mars, "Travel-time tomography in shallow water: Experimental demonstration at an ultrasonic scale," *The Journal of the Acoustical Society of America*, vol. 130, p. 1232, 2011.

[5] H. L. V. Trees, *Optimum Array Processing: Part IV of Detection, Estimation, and Modulation Theory*. Publishing House of Electronics Industry,, 2003.

[6] H. Krim and M. Viberg, "Two decades of array signal processing research: the parametric approach," *IEEE Signal Processing Magazine*, vol. 13, no. 4, pp. 67–94, 1996.

[7] R. Schmidt, "Multiple emitter location and signal parameter estimation," *Antennas and Propagation, IEEE Transactions on*, vol. 34, no. 3, pp. 276–280, 1986.

[8] H. Wang and M. Kaveh, "Coherent signal-subspace processing for the detection and estimation of angles of arrival of multiple wide-band sources," *Acoustics, Speech and Signal Processing, IEEE Transactions on*, vol. 33, no. 4, pp. 823–831, 1985.

[9] K. Buckley and L. Griffiths, "Broad-band signal-subspace spatial-spectrum (bass-ale) estimation," *Acoustics, Speech and Signal Processing, IEEE Transactions on*, vol. 36, no. 7, pp. 953–964, 1988.

[10] P. Gounon and S. Bozinoski, "High resolution spatio-temporal analysis by an active array," in *Acoustics, Speech, and Signal Processing, 1995. ICASSP-95., 1995 International Conference on*, vol. 5. IEEE, 1995, pp. 3575–3578.

[11] J. Evans, J. Johnson, and D. Sun, "High resolution angular spectrum estimation techniques for terrain scattering analysis and angle of arrival estimation," in *Proc. 1st ASSP Workshop Spectral Estimation*, 1981, pp. 134–139.

[12] J. Evans, "Application of advanced signal processing techniques to angle of arrival estimation in atc navigation and surveillance systems," DTIC Document, Tech. Rep., 1982.

[13] T. Shan, M. Wax, and T. Kailath, "On spatial smoothing for direction-of-arrival estimation of coherent signals," *Acoustics, Speech and Signal Processing, IEEE Transactions on*, vol. 33, no. 4, pp. 806–811, 1985.

[14] B. Rao and K. Hari, "Weighted subspace methods and spatial smoothing: Analysis and comparison," *Signal Processing, IEEE Transactions on*, vol. 41, no. 2, pp. 788–803, 1993.

[15] Y. Choi, "Subspace-based coherent source localisation with forward/backward covariance matrices," in *Radar, Sonar and Navigation, IEE Proceedings-*, vol. 149, no. 3. IET, 2002, pp. 145–151.

[16] E. Al-Ardi, R. Shubair, and M. Al-Mualla, "Computationally efficient high-resolution doa estimation in multipath environment," *Electronics Letters*, vol. 40, no. 14, pp. 908–910, 2004.

[17] R. Rajagopal and P. Rao, "Generalised algorithm for doa estimation in a passive sonar," in *Radar and Signal Processing, IEE Proceedings F*, vol. 140, no. 1. IET, 1993, pp. 12–20.

[18] K. Tan and G. Oh, "Estimating directions-of-arrival of coherent signals in unknown correlated noise via spatial smoothing," *Signal Processing, IEEE Transactions on*, vol. 45, no. 4, pp. 1087–1091, 1997.

[19] C. Qi, Y. Wang, Y. Zhang, and Y. Han, "Spatial difference smoothing for doa estimation of coherent signals," *Signal Processing Letters, IEEE*, vol. 12, no. 11, pp. 800–802, 2005.

[20] H. Wang and M. Kaveh, "On the performance of signal-subspace processing–part ii: Coherent wide-band systems," *Acoustics, Speech and Signal Processing, IEEE Transactions on*, vol. 35, no. 11, pp. 1583–1591, 1987.

[21] C. Paulus and J. Mars, "New multicomponent filters for geophysical data processing," *Geoscience and Remote Sensing, IEEE Transactions on*, vol. 44, no. 8, pp. 2260–2270, 2006.

[22] L. Jiang, F. Aulanier, G. Le Touze, B. Nicolas, and J. Mars, "Raypath separation with high resolution processing," in *OCEANS, 2011 IEEE-Spain*. IEEE, 2011, pp. 1–5.

[23] B. Cornuelle and B. M. Howe, "High spatial resolution in vertical slice ocean acoustic tomography," *Journal of Geophysical Research Atmospheres*, vol. 921, no. C11, pp. 11 680–11 692, 1987.

[24] E. K. Skarsoulis and B. D. Cornuelle, "Travel-time sensitivity kernels in ocean acoustic tomography," *Journal of the Acoustical Society of America*, vol. 116, no. 1, pp. 227–238, 2004.

[25] B. D. V. Veen and K. M. Buckley, "Beamforming: a versatile approach to spatial filtering," *IEEE Assp Magazine*, vol. 5, no. 2, pp. 4–24, 1988.

[26] M. Dzieciuch, P. Worcester, and W. Munk, "Turning point filters: Analysis of sound propagation on a gyre-scale," *The Journal of the Acoustical Society of America*, vol. 110, p. 135, 2001.

[27] Y. C. Eldar, A. Nehorai, and P. S. La Rosa, "A competitive mean-squared error approach to beamforming," *IEEE Transactions on Signal Processing*, vol. 55, no. 11, pp. 5143–5154, 2007.

[28] S. Srinivasan, A. Pandharipande, and K. Janse, "Beamforming under quantization errors in wireless binaural hearing aids," *EURASIP Journal on Audio, Speech, and Music Processing*, vol. 2008, no. 1, pp. 1–8, 2007.

[29] P. Stoica and N. Arye, "Music, maximum likelihood, and cramer-rao bound," *Acoustics, Speech and Signal Processing, IEEE Transactions on*, vol. 37, no. 5, pp. 720–741, 1989.

[30] P. Stoica and A. Nehorai, "Music, maximum likelihood, and cramer-rao bound: further results and comparisons," *Acoustics, Speech and Signal Processing, IEEE Transactions on*, vol. 38, no. 12, pp. 2140–2150, 1990.

[31] D. H. Johnson and D. E. Dudgeon, *Array Signal Processing: Concepts and Techniques.* Simon & Schuster, 1992.